

# Experimental Investigation of Emissivity of Aluminum Alloys and Temperature Determination Using Multispectral Radiation Thermometry (MRT) Algorithms

Chang-Da Wen and Issam Mudawar

(Submitted 9 April 2002; in revised form 22 May 2002)

Experiments were performed to measure the emissivity spectra for aluminum (Al) surfaces that are subject to variations in alloy, temperature, heating time, and surface finish. The linear emissivity model (LEM) and log-linear emissivity (LLE) model were tested against thermocouple measurements to explore the accuracy of these models at inferring surface temperature. The data show emissivity decreases with increasing wavelength for  $\lambda < 3.5 \mu\text{m}$ , but the trend is reversed at higher wavelengths. Except for AL 1100 (commercially pure Al), the emissivity of all alloys tested decreased 600-700 K and increased 700-800 K. The increased emissivity at 800 K was closely associated with a discoloration of surfaces from light gray into black. Surface roughness produced a 2- to 3-fold increase in emissivity compared with polished surfaces. Overall, the third-order LEM model showed the best overall accuracy for different alloys, temperatures, and surface roughness. Nonetheless, this study points to a need for more accurate models that could handle the diverse operating environment of Al processing plants.

**Keywords** aluminum, emissivity, temperature measurement

## 1. Introduction

### 1.1 Temperature Sensing Needs in Aluminum Processing

Aluminum (Al) alloy is undeniably the world's most important and most widely used lightweight metal. Its inherent attributes of high strength-to-weight ratio, corrosion resistance, relatively low-temperature production requirements, and recyclability have made Al the metal of choice for applications ranging from household window frames to structural members in commercial aircraft and military. Those same attributes have made possible the development of the so-called *aluminum intensive vehicles*, and there seems to be no shortage of new applications for this important metal.

Concurrent pressures of increased competitiveness and the requirements of superior mechanical properties, higher product quality, and lower cost are creating an urgent need to greatly improve production practices in the Al industry. Most Al fabrication processes require accurate determination of the Al alloy temperature at various stages of the process. For example, controlling the Al extrusion process demands temperature measurement during melting, casting, heating of billets, and profile pressing. The temperatures and rate of heating or cooling during a process influence metallurgical transformations, which ultimately have a strong impact on the mechanical properties of the final product. For instance, the cooling rate during profile pressing affects the optimum extrusion speed required to en-

sure desired mechanical properties. Overall, accurate temperature measurements help ensure product quality and reproducibility, as well as reduce cost by reducing scrap.

Contact temperature sensors such as thermistors and thermocouples are commonly used for temperature measurement in most industries. However, these types of sensors are undesirable in many Al processes because physical contact between a stationary sensor and a fast-moving metal surface may alter the surface physically or chemically. Furthermore, the contact temperature measurement methods currently in use in Al processing can achieve an accuracy no better than  $\pm 10\text{-}25 \text{ K}$ ,<sup>[1]</sup> which is below target for many Al fabrication processes.

### 1.2 Radiation Thermometry

Radiation thermometry is a convenient, noncontact method for temperature measurement of fast-moving Al surfaces. Radiation thermometers measure the intensity of thermal radiation from the target surface. Using fundamental electromagnetic wave theory, the measured intensity is used to infer the temperature of the surface when referenced to an ideal surface called a blackbody. The spectral intensity of radiation emitted by a blackbody at temperature  $T$  is given by the Planck distribution

$$L_{\lambda,b}(\lambda, T) = \frac{c_1}{\lambda^5 \left( e^{\frac{c_2}{\lambda T}} - 1 \right)} \quad (\text{Eq 1})$$

and  $c_1 = 1.19 \times 10^8 \text{ W} \cdot \mu\text{m}^4 \cdot \text{m}^{-2} \cdot \text{sr}^{-1}$  and  $c_2 = 1.439 \times 10^4 \mu\text{m} \cdot \text{K}$ .

The intensity of radiation emitted from a target surface is smaller than from a blackbody at the same temperature. A surface radiative property termed *emissivity* is defined as the ratio of intensity of radiation emitted by a surface at tempera-

Chang-Da Wen and Issam Mudawar, Boiling and Two-phase Flow Laboratory, School of Mechanical Engineering, Purdue University, West Lafayette, Indiana 47907. Contact e-mail: mudawar@ecn.purdue.edu.

ture  $T$  to that emitted by a blackbody at the same temperature. Spectral emissivity can therefore be expressed as

$$\varepsilon_\lambda(\lambda, T) = \frac{L_{\lambda,e}(\lambda, T)}{L_{\lambda,b}(\lambda, T)} \quad (\text{Eq 2})$$

The spectral intensity measured by a radiation thermometer,  $L_{\lambda,meas}$ , consists of four components,

$$L_{\lambda,meas}(\lambda, T) = L_{\lambda,e}(\lambda, T) + L_{\lambda,ref} + L_e + L_s \quad (\text{Eq 3})$$

where  $L_{\lambda,e}$  is the intensity of radiation emitted from the target,  $L_{\lambda,ref}$  is the intensity of irradiation from the surroundings that is

reflected by the target surface,  $L_e$  is the target emission reflected by the surrounding onto the target itself, and  $L_s$  is the combined effect of atmospheric scattering and absorption ( $\text{H}_2\text{O}$ ,  $\text{CO}_2$ , dust particles, etc). If the target area is small compared with the surroundings, the surroundings will behave as a large blackbody enclosure that absorbs all incoming radiation, and  $L_e$  becomes negligible. The atmospheric scattering term  $L_s$  is important only over narrow wavelength bands and negligible elsewhere. Outside these scattering bands, the measured intensity of a small target can be simplified as

$$L_{\lambda,meas}(\lambda, T) \cong L_{\lambda,e}(\lambda, T) + L_{\lambda,ref} = \varepsilon_\lambda L_{\lambda,b}(\lambda, T) + \rho_\lambda L_{\lambda,b}(\lambda, T_{sur}) \quad (\text{Eq 4})$$

where  $\rho_\lambda$  is the spectral reflectivity of the target surface, or fraction of the intensity of irradiation from the surroundings (at  $T_{sur}$ ) that is reflected by the target surface. Applying energy conservation and Kirchhoff's law for an opaque surface gives

$$\rho_\lambda = 1 - \varepsilon_\lambda \quad (\text{Eq 5})$$

Combining Eq 4 and 5 yields the following popular expression for the measured radiation intensity of an opaque target surface,

$$L_{\lambda,meas}(\lambda, T) = \varepsilon_\lambda L_{\lambda,b}(\lambda, T) + (1 - \varepsilon_\lambda) L_{\lambda,b}(\lambda, T_{sur}) \quad (\text{Eq 6})$$

where  $L_{\lambda,b}(\lambda, T)$  and  $L_{\lambda,b}(\lambda, T_{sur})$  can be calculated from the Planck distribution, Eq 1. Equation 6 enables the determination of the target surface temperature  $T$  from the measured spectral intensity  $L_{\lambda,meas}$ , provided  $\varepsilon_\lambda$  is known.

For a hot target surface in low temperature surroundings,  $L_{\lambda,b}(\lambda, T) \gg L_{\lambda,b}(\lambda, T_{sur})$  and the second term on the right-hand-side of Eq 6 can be neglected without compromising measurement accuracy. As will be discussed later, this may not always be true in an AI production environment.

Three categories of radiation thermometry methods are commonly used in conjunction with Eq 6 to infer the target surface temperature: spectral, dual-wavelength, and multispectral. They differ by the number of wavelengths at which the radiation intensity is measured. Spectral radiation thermometry is based on intensity measurement at one wavelength and a constant emissivity value independent of wavelength. Dual-wavelength radiation thermometry (DWRT) uses intensity measurements at two distinct wavelengths and an emissivity compensation algorithm to infer the surface temperature. Multispectral radiation thermometry (MRT) employs intensity measurements at three or more wavelengths and a multi-wavelength emissivity model to determine the surface temperature. The MRT method is preferred for its ability to enhance measurement accuracy as well as account for the complex spectral variations of both radiation intensity and emissivity.

### 1.3 Emissivity Models

The emissivity models used in Eq 6 to determine the target surface temperature consist of either 1) mathematical functions whose coefficients are determined empirically from radiation intensity measurements at different wavelengths, or 2) analytical functions based on fundamental physical premises (e.g.,

Nomenclature	
$a_i$	unknown coefficient in emissivity models
$c_1$	first thermal radiation constant
$c_2$	second thermal radiation constant
$L_e$	spectral intensity of target surface emission reflected back by surroundings
$L_s$	spectral intensity of radiation associated with scattering and absorption
$L_{\lambda,b}$	spectral intensity of blackbody radiation
$L_{\lambda,e}$	spectral intensity of radiation emitted by target surface
$L_{\lambda,gen}$	generated spectral intensity of radiation given by Eq 10
$L_{\lambda,meas}$	measured spectral radiation intensity
$L_{\lambda,ref}$	spectral intensity of irradiation from surroundings that is reflected by target surface
MRT	Multispectral Radiation Thermometry
$n$	order of polynomial in emissivity model
$N$	number of wavelengths used in measurement or temperature inference
$T$	surface temperature
$T_{sur}$	temperature of surroundings
Greek Symbols	
$\varepsilon_\lambda$	spectral emissivity
$\lambda$	wavelength
$\rho_\lambda$	spectral reflectivity
$\chi_{LEM}^2$	least-squares error using LEM model in conjunction with MRT method
$\chi_{LLE}^2$	least-squares error using LLE model in conjunction with MRT method
Subscripts	
$b$	blackbody
$e$	emitted
$gen$	generated
$LEM$	linear emissivity model
$LLE$	log-linear emissivity model
$meas$	measured
$ref$	reflected
$sur$	surroundings
$\lambda$	spectral

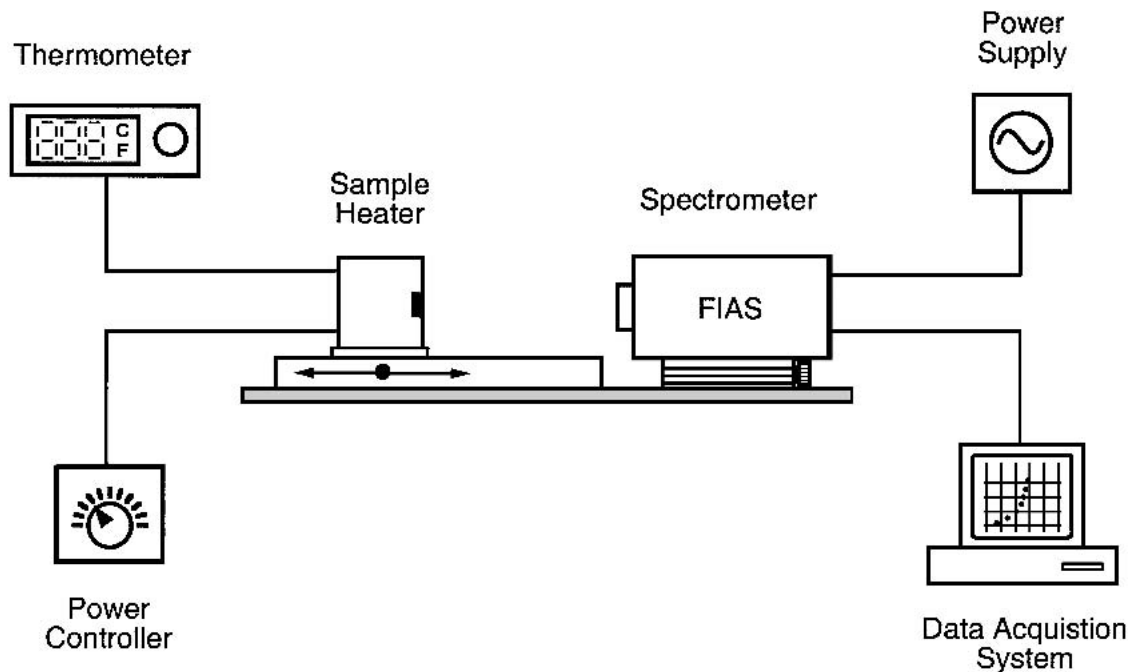


Fig. 1 Temperature measurement facility

Table 1 Al Alloys Tested in Present Study

Alloy	Constituents	Application	Heat Treatability?
AL 1100	0.12% Cu	Foils, claddings, surface finishings, sheet metal, spun hollow ware, and decorative parts	No
AL 2024	4.4% Cu, 1.5% Mg, and 0.6% Mn	Aircraft structures, truck wheels, and domestic products	Yes
AL 3104	1.1% Mn, 1.0% Mg, and 0.6% Cu	Beverage cans	No
AL 7075	5.6% Zn, 2.5% Mg, 1.6% Cur, and 0.23% Cr	Aircraft structures, keys, and alclad product surfaces	Yes
AL 7150	6.4% Zn, 2.4% Mg, 2.2% Cu, and 0.12% Zr	Aircraft structures	Yes

Maxwell, Hagen-Rubens, and Edwards models<sup>[2,3]</sup>). The coefficients in both types of emissivity models enable the MRT methods to depict the complex spectral emissivity characteristics of different target surface materials. Moreover, the increased number of wavelengths in the MRT method facilitates statistical reduction of temperature errors from measurement noise.

Two different mathematical techniques are used in conjunction with the MRT method: the exact technique and the least-squares technique. The exact technique utilizes an emissivity model with  $N$  unknown coefficients, and radiation intensity measurements at  $N + 1$  wavelengths. Applying Eq 6 for each intensity measurement results in  $N + 1$  equations with  $N + 1$  unknowns: the target surface temperature  $T$ , and the  $N$  unknown coefficients in the emissivity model. Coates<sup>[4]</sup> and Doloresco<sup>[5]</sup> suggested the exact technique might cause overfitting and result in large errors when used with more than three wavelengths.

The least-squares technique involves fitting of radiation intensity measurements at several wavelengths to simultaneously deduce the spectral emissivity and temperature of the target surface. This technique, which can overcome the overfitting

problem, is commonly used in MRT and has been recommended by many researchers. When using an emissivity model with  $N$  unknown coefficients, the least-squares technique demands spectral intensity measurements at a minimum of  $(N + 2)$  wavelengths. Two of the most popular MRT emissivity compensation models are the linear emissivity model (LEM)<sup>[5-15]</sup> and the log-linear emissivity model (LLE).<sup>[17,8,16-20]</sup>

Al alloys pose several serious challenges to the implementation of the MRT method. First, the low emissivity values of Al surfaces produce inherently weak intensity signals, which, as Eq 6 indicates, may lead to large errors when inferring the target surface temperature. Second, the high reflectivity of Al surfaces produces large sensitivity to irradiation from the surroundings, which can be at elevated temperatures in an Al production environment and, according to Eq 6, contribute measurable irradiation effects, which cannot always be accurately accounted for. Third, the emissivity of Al surfaces is a complex function of wavelength, temperature, alloy, surface finish (roughness and oxidation), thermal history, environment, and process conditions. But most importantly, these effects are not well understood, nor are there sufficient reliable published data for formulation of comprehensive emissivity algorithms.

The current study was conducted to better understand the interdependent parametric influences of temperature, heating time, alloy, and surface roughness on the spectral emissivity of Al surfaces. Spectral intensity was measured for a large number of samples encompassing all of these parameters, and used to infer the surface temperatures via the MRT method and different emissivity algorithms. The inferred temperature was compared with the temperature measured by a thermocouple embedded in the sample. Two popular MRT emissivity compensation models, the LLE model and the LEM model, are examined for accuracy in temperature determination subject to the aforementioned parametric influences. The goal here is to assess the versatility of emissivity models at representing the complex environment in Al processing facilities.

## 2. Experimental Methods

### 2.1 Test Apparatus

As shown in Fig. 1, the main components of the test apparatus for this study consisted of a spectrometer (radiation thermometer), test sample heating assembly, digital thermometer, and data acquisition system. Most of the apparatus was mounted atop a welded steel cart.

The radiation intensity measurements were made using a Fast IR Array Spectrometer (FIAS) Model ES100 made by Spectraline (West Lafayette, IN). This spectrometer is capable of measuring simultaneously 160 spectral radiation intensity values for discrete wavelengths ranging from 1.8-4.9  $\mu\text{m}$ . The radiation from the target (sample) surface incident on the entrance port of the FIAS is split into spectral components, and then dispersed over a staggered 160 element linear array PbSe detector. The voltages and pixel numbers provided by the linear array are converted into wavelengths and intensities using pre-installed calibration curves. The entrance port is a 5 mm  $\times$  1 mm slit, which creates a 35  $\mu\text{m}$  wide image on the array detector. The FIAS accepts incident radiation through an angle diverging  $\pm 0.25^\circ$  from the edges of the slit. For example, a target placed 150 mm from the entrance port (typical of the present measurements) will have the longest side of the target area of 6.31 mm ( $5 + 2 \times 150 \times \tan 0.25$ ). An alignment HeNe laser is used to point the spectrometer at a precise location on the target surface. To record and process the data, a computer and two ISA boards are used: a 1 MHz, 12 bit A/D board and a 32 MB memory board. The data acquisition is controlled by a drive circuit in the spectrometer itself. A Windows-based graphical user interface (GUI) is used for basic spectrometric functions that permit different output formats. The output can be either displayed on the GUI or stored in computer memory for later analysis.

The Al test sample was mounted against the exterior of an Al heating block as shown in Fig. 2. The heating block was used to raise the sample temperature to the desired test value. The heating block contained four cartridge heaters whose power was controlled by a variable voltage transformer. The entire heating assembly was encased in a thick blanket of Cotronics (Brooklyn, NY) high-temperature ceramic fiber insulation. The test sample was pressed against the heating block with the aid of solid flange made from low conductivity alu-

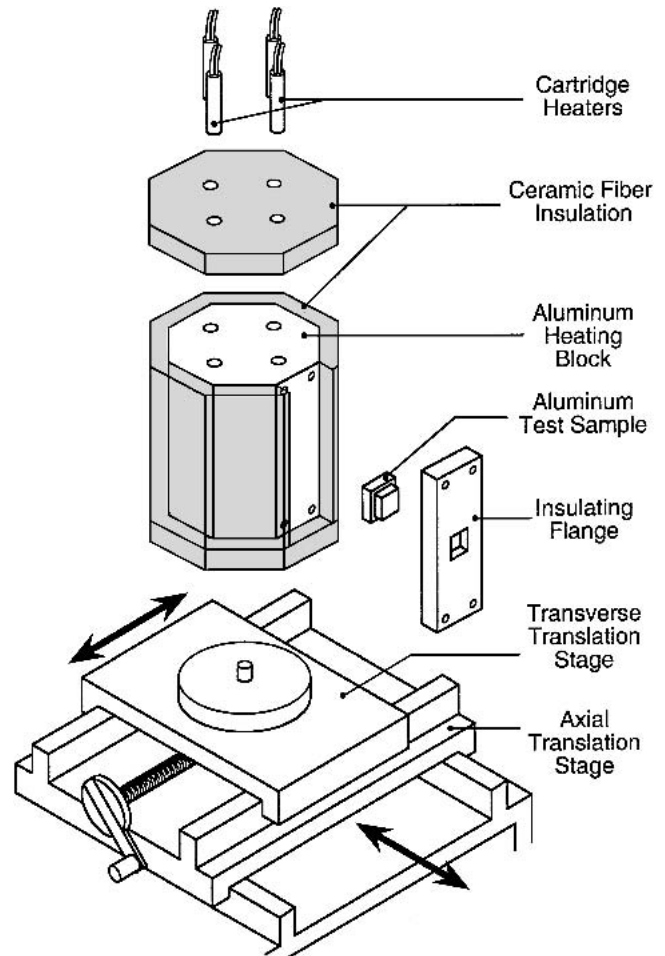


Fig. 2 Construction of sample heating assembly

Table 2 Polishing Procedure for Al Samples

Wheel Number	Abrasive and Size	Wheel Covering	Lubricant
1	SiC, 320 grit, 35 $\mu\text{m}$	Carbimet	Water
2	SiC, 400 grit, 22 $\mu\text{m}$	Carbimet	Water
3	SiC, 600 grit, 14 $\mu\text{m}$	Carbimet	Water
4	Diamond, 6 $\mu\text{m}$	Nylon cloth	Automet lapping oil
5	Gamma alumina, 0.05 $\mu\text{m}$	Microcloth	Distilled water

mina silicate. The entire heating assembly rested on a two-dimensional translation stage as illustrated in Fig. 2.

Figure 3 shows the detailed construction of the test sample and insulating flange. The exposed surface area of the sample is 15 mm  $\times$  15 mm. A thermocouple hole is drilled from the back of the sample to a distance of 1 mm from the surface. Accounting for both natural convection and radiation effects, the temperature gradient between the Omega Chromel-Alumel (type K) thermocouple bead (Stamford, CT) and sample surface is estimated at less than 0.03  $^\circ\text{C}$ , owing to both the high conductivity of Al and low heat flux supplied to the sample from the heating block. An Omega Model CL1000 hot point calibrator (Stamford, CT) was used to calibrate the thermo-

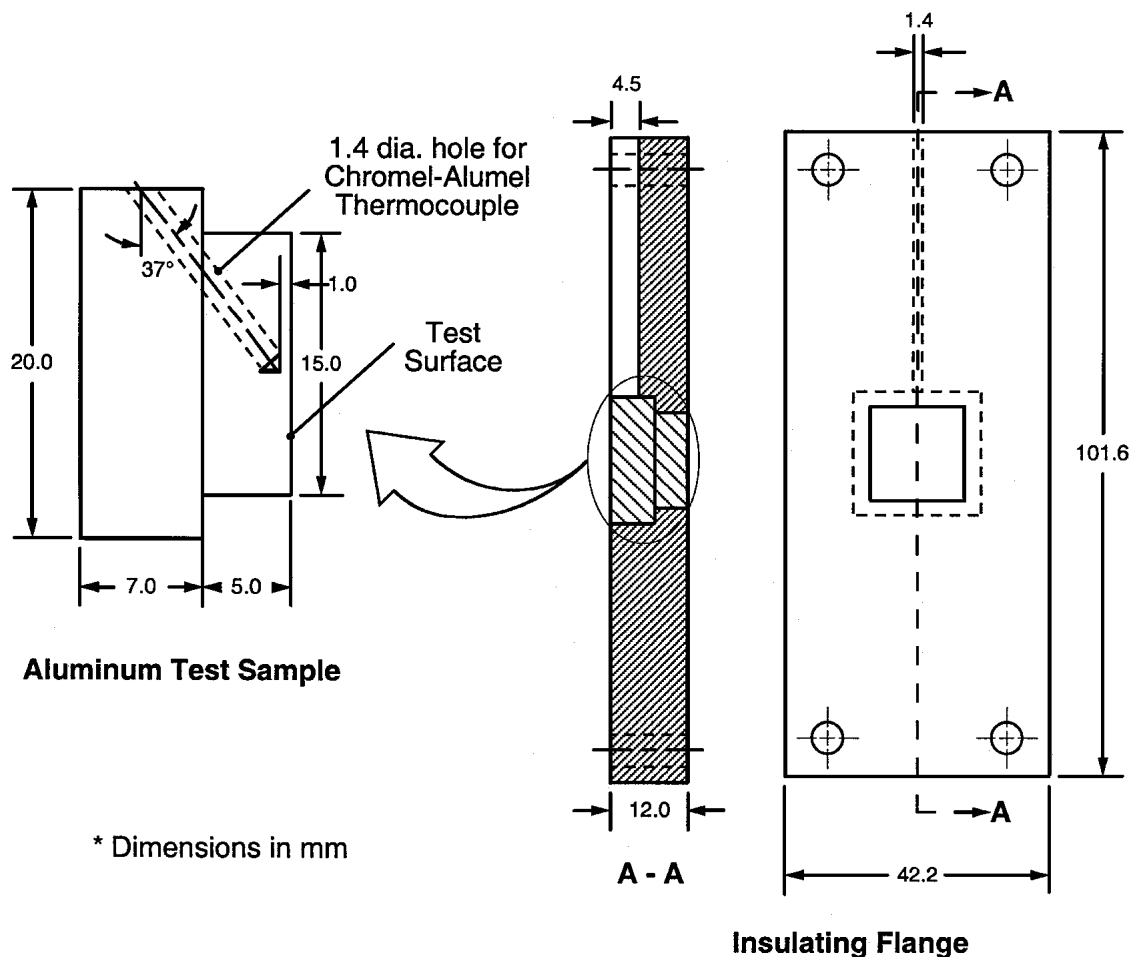


Fig. 3 Construction of Al test sample and insulating flange

couple output. The thermocouple readout from an Omega digital thermometer (Stamford, CT) was corrected for the calibration offset, which was typically less than 1.6 °C for a surface temperature of 523 K.

Test samples encompassing a variety of Al alloys and surface finishes were tested. Table 1 shows major constituents, applications, and the heat-treatability of the five alloys that were tested. The commercially pure AL 1100 is a nonheat-treatable metal that has little practical use, but is investigated as a comparative reference for all Al alloys.

Five different types of surface finish were examined: polished, 6 μm roughened, 14 μm roughened, extruded, and saw-cut. Figure 4 shows representative SEM images of AL 7075 samples with the five different surface finishes. The polished surface was created by successive use of five polishing wheels with increasingly finer grit as detailed in Table 2. Scratches remaining on this mirror-like surface were no wider than 0.05 μm. The 6 μm samples were cut and milled to size before being rubbed with cloth on a polishing wheel containing 6 μm diamond compound. The 14 μm samples were fabricated in the same manner but later roughened with Hudson Carborundum 600 grit paper (Cleveland, OH). The extruded and saw-cut samples were supplied directly from the Aluminum Company of America (ALCOA), Lafayette, IN, and machined to size.

Great care was exercised during the cutting and milling of those samples to preserve their original surface finish. The average surface roughness of the extruded samples ranged from 0.1-0.5 μm. The saw-cut samples were cut at ALCOA from Al bar or ingot. The average surface roughness of the saw-cut samples was highly directional, ranging from 4-12 μm across, and 0.15-2.14 μm along the sawing direction, respectively.

## 2.2 Experimental Procedure

After the samples were cut and milled to size, the test surface was cleaned with acetone followed by methanol to remove any oils, grease, or dirt. The samples were handled with great care and wrapped in fine tissue to make certain their surfaces were free from contact with roughening agents following the surface preparation.

Initially, the heating block was preheated to a temperature slightly above the desired value. Next, the Type K thermocouple was inserted into the sample's thermocouple hole, which was pre-packed with high thermal conductivity boron nitride powder, ensuring good thermal contact between the thermocouple bead and sample. The sample was then mounted onto the outer surface of the preheated block and held in place

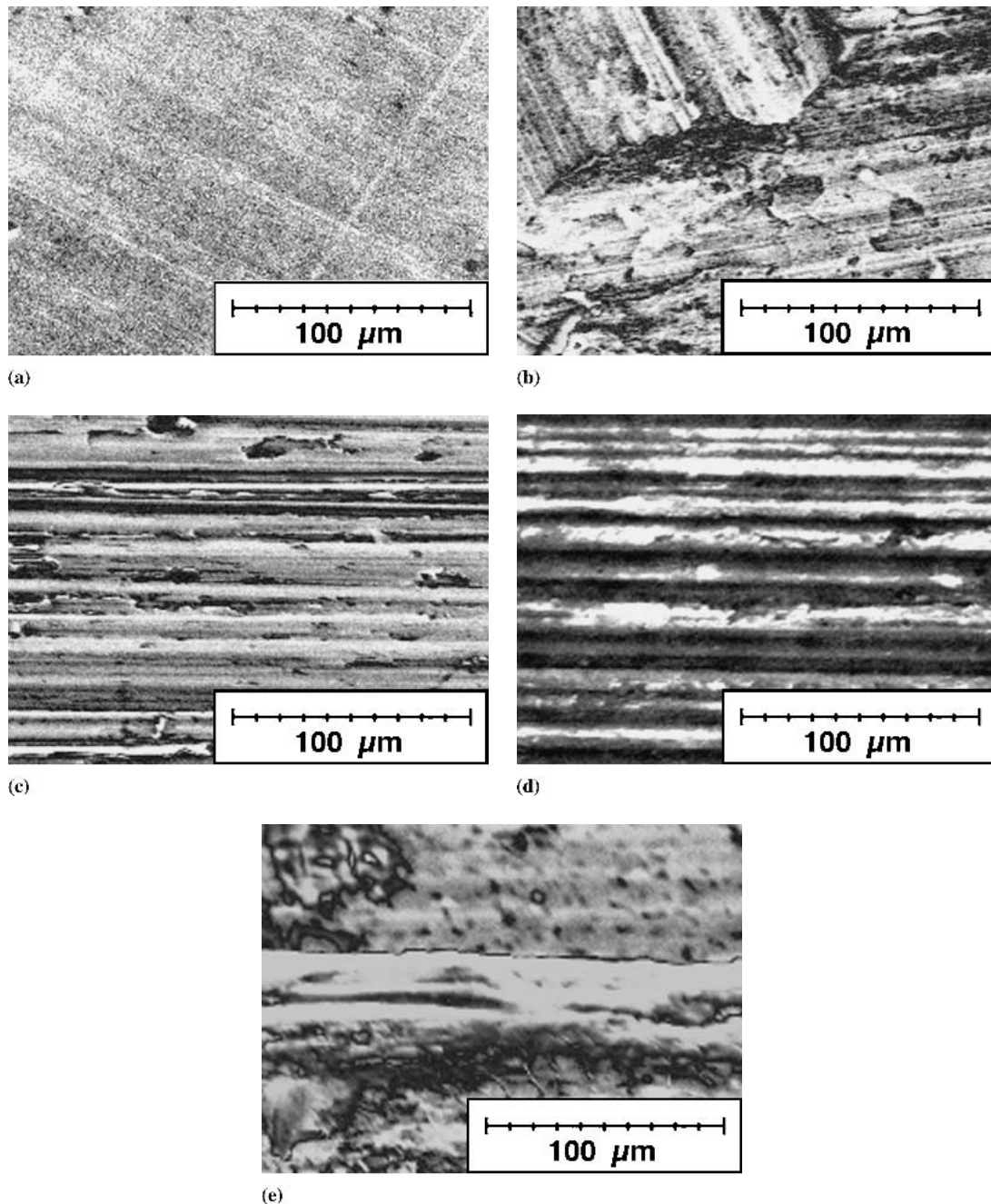
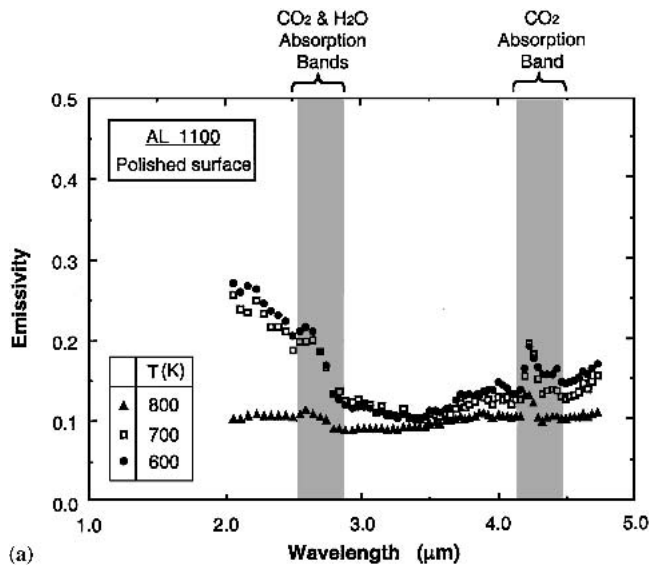


**Fig. 4** Scanning electron microscope images of AL 7075 sample surfaces: (a) polished; (b) roughened with 6  $\mu\text{m}$  diamond compound; (c) roughened with 14  $\mu\text{m}$  grit paper; (d) extruded; (e) saw-cut

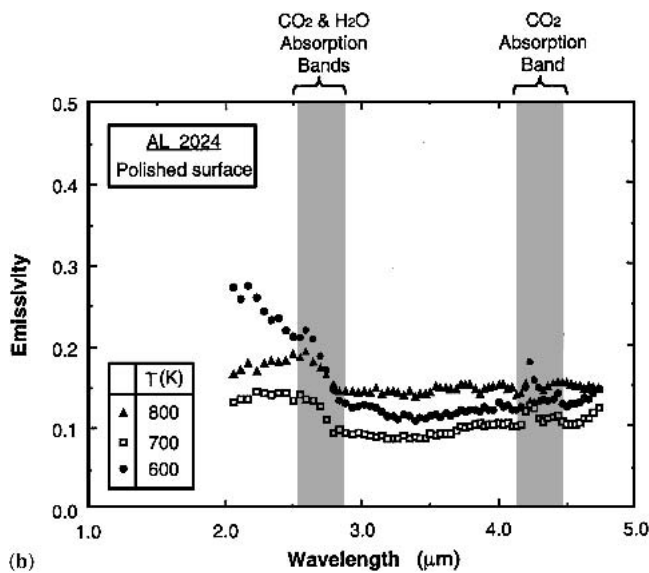
with the aid of the insulating flange. This initiated heat-up of the test sample. The desired sample temperature was achieved by manipulating power input to the cartridge heaters using the variable voltage transformer. Both the thermocouple and spectrometer data were ready to be collected once the temperature of the sample reached steady state.

The spectrometer was aligned by focusing on a HeNe laser spot aimed at the center of the sample surface. The spectral intensity data were collected by the spectrometer and stored at 390 Hz. At the same time, the sample thermocouple output was

measured by the digital thermometer and recorded manually. For this study, three temperatures, 600, 700, and 800 K, were selected for measurement and analysis because of the importance of this temperature range to Al heat treating. All the experiments were performed in a normal laboratory environment with a fairly constant room temperature around 295 K. After the measurements were completed, power to the heating block and spectrometer was shut off, and the test sample was removed from the heating block and allowed to cool down to room temperature.



(a)



(b)

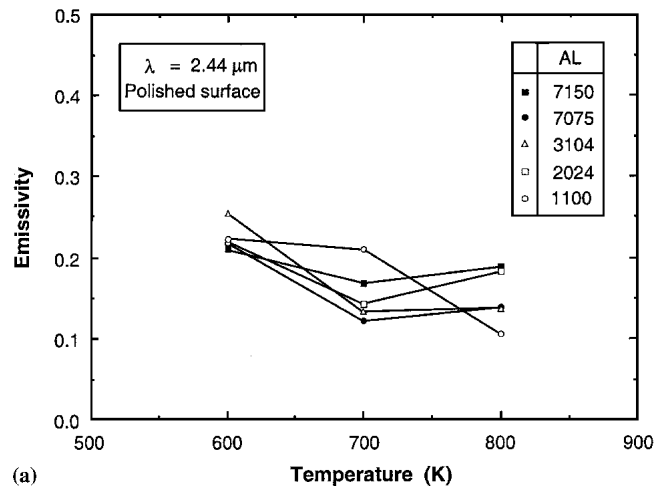
Fig. 5 Effects of temperature on spectral emissivity for (a) AL 1100 and (b) AL 2024

### 3. Results and Discussion

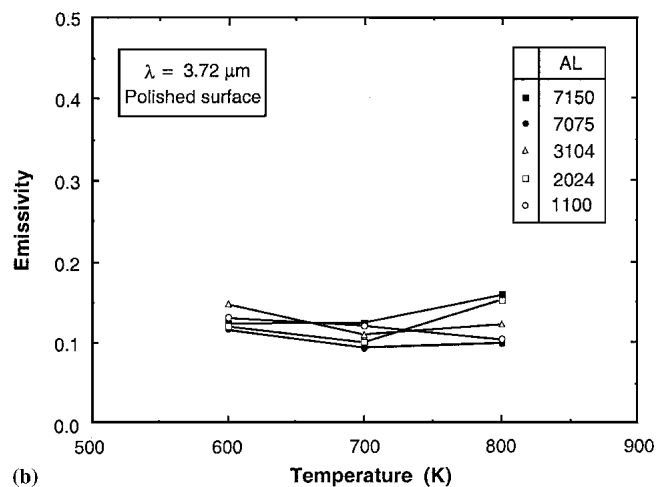
Spectral emissivity was measured for samples encompassing the five Al alloys and five surface finishes. The spectral emissivity was calculated for each wavelength using Eq 6, where  $L_{\lambda, meas}$  was measured by the spectrometer, and  $L_{\lambda, b}(\lambda, T)$  and  $L_{\lambda, b}(\lambda, T_{sur})$  were calculated from the Planck distribution, Eq 1, using the sample temperature  $T$  measured by the thermocouple and the room temperature  $T_{sur}$ , respectively. Below is a discussion of the effects of sample temperature, heating time, alloy, and surface roughness on the spectral emissivity.

#### 3.1 Temperature Effects

Figure 5(a) and (b) show the spectral emissivity distribution for AL 1100 and AL 2024 samples with polished surfaces at surface temperatures of 600, 700, and 800 K and  $2.00 < \lambda <$



(a)



(b)

Fig. 6 Effects of temperature on spectral emissivity at wavelengths of (a) 2.44  $\mu\text{m}$  and (b) 3.72  $\mu\text{m}$

4.72  $\mu\text{m}$ . The two shaded areas in each figure represent the atmospheric absorption and scattering bands which, according to Eq 3, influence the intensity measurement and cause errors in calculating the spectral emissivity using Eq 6. The first band, which is centered around 2.7  $\mu\text{m}$ , is due to radiation caused by H<sub>2</sub>O (room humidity) and CO<sub>2</sub> molecules, and the second, centered around 4.3  $\mu\text{m}$ , is due to CO<sub>2</sub> molecules alone. Figure 5(a) and (b) show the spectral emissivity distribution for different Al alloys with polished surfaces is somewhat different from those of other metallic surfaces. For most metallic surfaces, spectral emissivity increases with decreasing wavelength and increasing temperature.<sup>[21]</sup> The present data exhibit a decreasing emissivity with increasing wavelength for  $\lambda < 3.5 \mu\text{m}$ , but the trend is reversed at higher wavelengths. The emissivity of AL 1100 actually decreases with increasing temperature, while for AL 2024, emissivity decreases between 600 and 700 K and increases between 700 and 800 K. Except for AL 1100 at 800K, the two different alloys retain a similar overall shape of emissivity distribution, though their magnitudes are different due to the differences in composition.

Figure 6(a) and (b) shows the spectral emissivity variations with temperature for all five alloys at  $\lambda = 2.44$  and 3.72  $\mu\text{m}$ ,

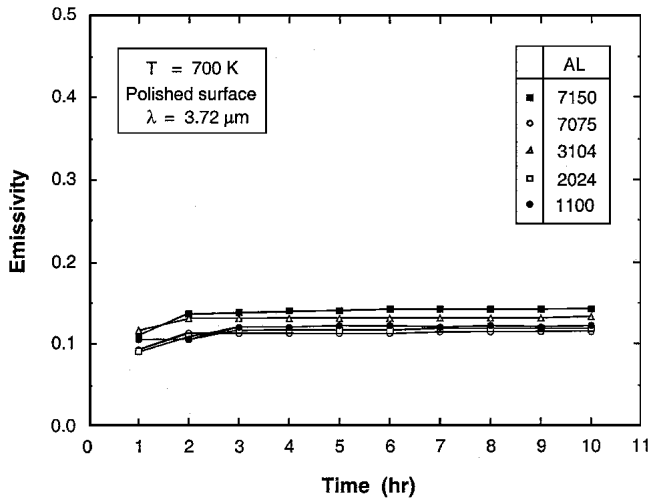


Fig. 7 Effects of heating time on spectral emissivity

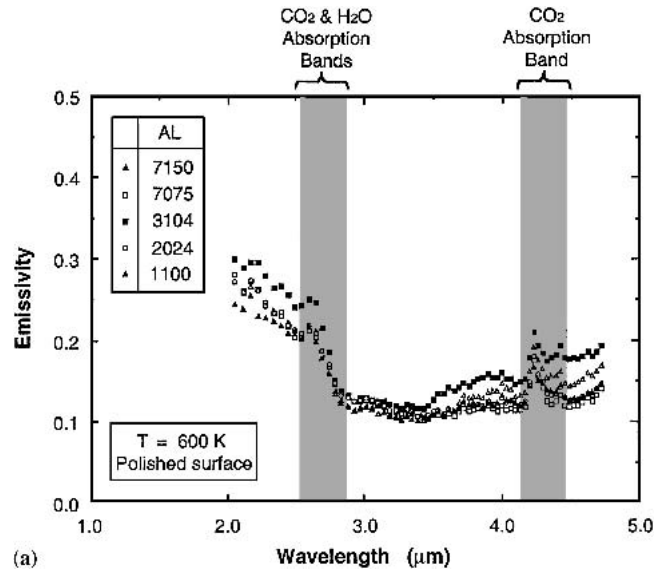
respectively. Except for AL 1100 (commercially pure Al), the emissivity trends for all alloys are similar, decreasing first between 600 and 700 K and then increasing above 700 K. For AL 1100, the spectral emissivity decreases monotonically with increasing temperature. The increased spectral emissivity for all the other alloy surfaces at 800 K was observed to be closely associated with surface discoloration. The surface color of these magnesium-containing alloys turned during heating from light gray into black, which helped increase emissivity as suggested in previous studies.<sup>[22]</sup> This discoloration was observed at 800 K on every alloy sample, but not on AL 1100.

### 3.2 Effects of Heating Time

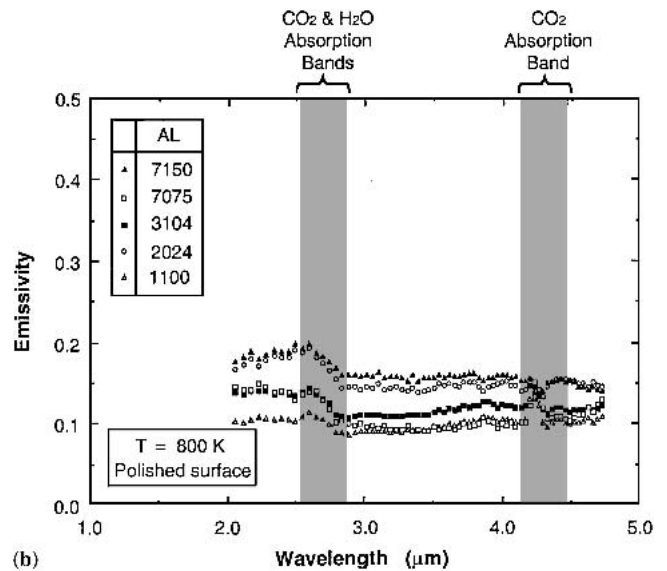
Previous studies have shown that spectral emissivity increases when an Al alloy is held at an elevated temperature for a long duration, and this increase is generally attributed to surface oxidation.<sup>[23,24]</sup> Figure 7 shows the effects of heating time on spectral emissivity for the present samples. All the oxidation effects seem to be concentrated in the initial three hours. This effect is much smaller for AL 1100 than for the alloys. Oxidation on the alloy surfaces seems to attain some consistent surface composition after 3 h. There is also a slight increase in spectral emissivity after 10 h. This is consistent with trends reported by previous investigators.<sup>[20,23,24]</sup> Future studies on the effects of oxidation should therefore be focused on the initial heating time. Such studies may lead to useful relationships between spectral emissivity and initial oxidation rate.

### 3.3 Effects of Alloy

Figure 8(a) and (b) illustrate the complex effects of alloy on the spectral emissivity of polished samples at 600 and 800 K, respectively. Figure 8(a) shows emissivity values at 600 K converge for  $2.7 < \lambda < 3.5 \mu\text{m}$ . A much stronger alloy effect is evident at the higher temperature. Also at 800 K, the emissivity of AL 1100 is lowest of all samples over the entire spectral domain. This lends credence to the aforementioned oxidation



(a)



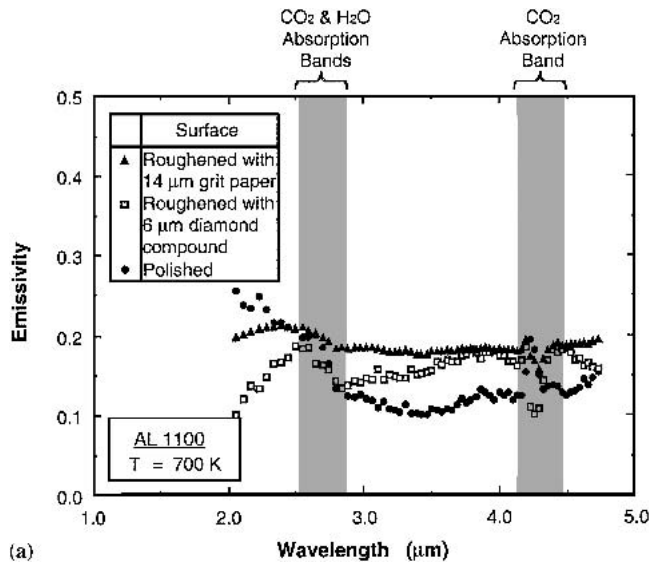
(b)

Fig. 8 Effect of alloy on spectral emissivity at temperatures of (a) 600 K and (b) 800 K

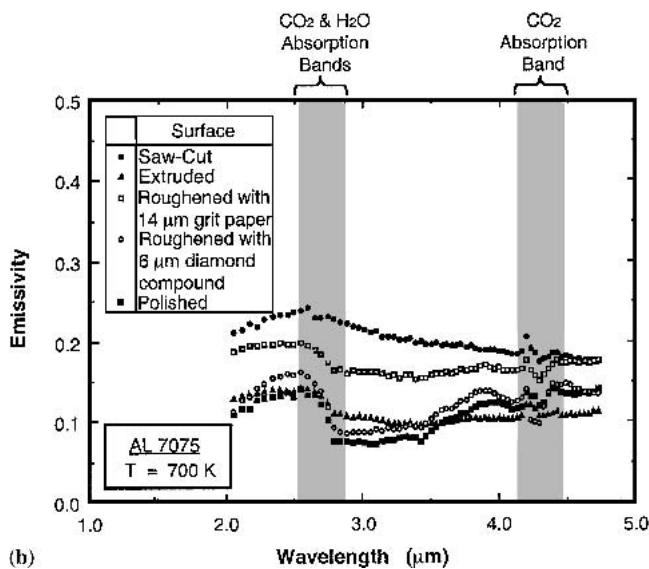
hypothesis since oxidation, which was prevalent on the other alloy samples, was far more pronounced at 800 K.

### 3.4 Effects of Surface Roughness

Figure 9(a) and (b) show the effects of surface roughness on spectral emissivity for AL 1100 and AL 7075, respectively. In the first figure, an increase in the roughness of AL 1100 produces a monotonic increase in spectral emissivity, except for  $\lambda < 2.7 \mu\text{m}$ . Surface roughening also appears to alter the shape of the spectral emissivity distribution substantially. The same trend is observed with AL 7075, but with a far more pronounced roughness effect, manifest by a 2- to 3-fold increase in emissivity for the saw-cut surface compared with the polished surface. For both AL 1100 and AL 7075, the emissivity distribution appears to become flatter with increasing roughness.



(a)



(b)

**Fig. 9** Effects of surface roughness on spectral emissivity for (a) AL 1100 and (b) AL 7075

The complex changes in spectral emissivity distribution resulting from temperature, alloy, and roughness illustrate the difficulty in developing universal emissivity models that can be used throughout the Al industry.

#### 4. Application of MRT Emissivity Models

The least-squares technique is used in this study to simultaneously deduce the best-fit values of emissivity and temperature when a particular form of spectral emissivity (i.e., emissivity algorithm) is assumed. The number of unknown coefficients in the emissivity model must be at least two less than the number of spectral intensity values.

Two of the most commonly used MRT mathematical emissivity models are examined. They are the previously mentioned LEM and the LLE models.

The LEM model,

$$\varepsilon_\lambda = a_0 + a_1\lambda + a_2\lambda^2 + \dots + a_n\lambda^n \quad (\text{Eq 7})$$

is a polynomial function of wavelength, which has been used by many investigators to examine a broad variety of surface materials.<sup>[5-15]</sup>

The LLE model,

$$\varepsilon_\lambda = \exp(a_0 + a_1\lambda + a_2\lambda^2 + \dots + a_n\lambda^n) \quad (\text{Eq 8})$$

is the exponential of a polynomial function of wavelength. This model was also studied and used extensively by many researchers.<sup>[7,8,16-20]</sup>

For an  $n$ th power polynomial in both the LEM and LLE models, the number of unknown empirical constants in the emissivity model is  $N = n + 1$ . Using measurements at  $N + 1$  (or  $n + 2$ ) wavelengths will facilitate the use of the exact MRT method to determine all the emissivity coefficients as well as the surface temperature  $T$ . The least-squares method used in the current study will require a minimum of  $N + 2$  (or  $n + 3$ ) wavelengths<sup>[18,19]</sup> to determine the emissivity coefficients and  $T$ .

For the LLE model, Gardner,<sup>[9]</sup> Doloresco,<sup>[5]</sup> and Gathers<sup>[18,19]</sup> all concluded that no measurable error reduction in the inferred surface temperature would be realized by increasing the number of wavelengths used beyond the minimum required when employing the least-squares technique. In addition, Coates<sup>[4]</sup> has shown there is no benefit to increasing the number of unknown coefficients in emissivity models. In other words, using a much higher order polynomial is not recommended.

For the LEM, the rationale of the least-squares technique is to determine the inferred surface temperature and the unknown emissivity coefficients by minimizing the magnitude of  $\chi_{LEM}^2$  in the following equation

$$\chi_{LEM}^2 = \sum_{i=0}^n (L_{\lambda,meas,i} - L_{\lambda,gen,i})^2 \quad (\text{Eq 9})$$

where  $L_{\lambda,meas,i}$  and  $L_{\lambda,gen,i}$  are the measured and generated values of spectral intensity, respectively. Neglecting the intensity of irradiation from the surroundings which is reflected by the target surface, the generated spectral intensity can be expressed as

$$L_{\lambda,gen}(\lambda, T) \equiv \varepsilon_\lambda(\lambda) L_{\lambda,b}(\lambda, T) = \varepsilon_\lambda(\lambda) \frac{c_1}{\lambda^5 \left( e^{\frac{c_2}{\lambda T}} - 1 \right)} \quad (\text{Eq 10})$$

For the LLE model, the least-squares technique is used to determine the inferred temperature and the unknown emissivity coefficients by minimizing the magnitude of  $\chi_{LLE}^2$  in the following equation

$$\chi_{LLE}^2 = \sum_{i=0}^n (\ln L_{\lambda,meas,i} - \ln L_{\lambda,gen,i})^2 \quad (\text{Eq 11})$$

**Table 3 Mathematical Form of LLE Model and LEM Model Examined in This Study**

Emissivity Model	Mathematical Function	Polynomial Order	Required Minimum Number of Wavelengths
LLE	$\epsilon_\lambda = \exp(a_0 + a_1\lambda)$	1	4
	$\epsilon_\lambda = \exp(a_0 + a_1\lambda + a_2\lambda^2)$	2	5
	$\epsilon_\lambda = \exp(a_0 + a_1\lambda + a_2\lambda^2 + a_3\lambda^3)$	3	6
LEM	$\epsilon_\lambda = a_0 + a_1\lambda$	1	4
	$\epsilon_\lambda = a_0 + a_1\lambda + a_2\lambda^2$	2	5
	$\epsilon_\lambda = a_0 + a_1\lambda + a_2\lambda^2 + a_3\lambda^3$	3	6

Given is the order of polynomial used in each model and minimum number of wavelengths required when using the least-squares technique.

**Table 4 Absolute Errors in Inferred Temperature of Al Alloys for Different Surface Roughness and Different Spectral Ranges at 600 K Using the LLE Model and LEM Model**

Surface Condition	Emissivity Model	Polynomial Order	Wavelength, $\mu\text{m}$								
			2.05-3.43			3.50-4.72			2.05-4.72		
			AL 1100	AL 2024	AL 7150	AL 1100	AL 2024	AL 7150	AL 1100	AL 2024	AL 7150
Polished	LLE	1	6.5	20.4	-32.9	...	...	...	...	...	...
		2	...	...	...	...	...	...	...	...	...
		3	...	...	...	...	...	...	...	...	...
	LEM	1	...	...	...	...	...	...	-11.2	41.0	18.8
		2	...	...	...	...	...	...	...	...	...
		3	34.2	-45.7	-13.6	...	...	...	...	...	...
Roughened with 14 $\mu$ grit paper	LLE	1	...	...	13.5	...	...	...	...	...	...
		2	...	...	...	...	...	...	...	...	...
		3	...	...	...	...	...	...	...	...	...
	LEM	1	...	...	...	...	...	...	...	38.7	...
		2	-42.6	-36.0	...	...	...	...	...	...	...
		3	-5.3	-24.9	-28.1	-26.6	...	...	37.7	25.2	29.0

Missing values correspond to errors beyond  $\pm 50$  K.

When used in conjunction with the LLE model, Eq 10 is first simplified by approximating the Planck blackbody distribution by Wien’s formula,

$$L_{\lambda,b}(\lambda, T) = \frac{c_1}{\lambda^5 \left( e^{\frac{c_2}{\lambda T}} - 1 \right)} \cong \frac{c_1}{\lambda^5 \left( \frac{c_2}{\lambda T} \right)} \quad (\text{Eq 12})$$

This provides a set of equations, which are linear with respect to the inferred temperature and the unknown emissivity coefficients.

Table 3 shows the mathematical form of the LLE and LEM models examined in this study, along with the order of polynomial function used, and minimum number of required wavelengths incorporated in the least squares technique. Errors in the inferred temperature are given in Tables 4 and 5 for surface temperatures of 600 and 700 K, respectively. Each table includes results for three Al alloys, AL 1100, AL 2024, and AL 7150, and both polished and 14  $\mu\text{m}$  roughened surfaces. The results are shown for a short range of the measurement wavelengths 2.05-3.43  $\mu\text{m}$ , a long range 3.50-4.72  $\mu\text{m}$ , and the combined range 2.05-4.72  $\mu\text{m}$ . Polynomial functions up to third order are examined with both models. The third order is generally the upper limit in application of the LEM model and is adequate at representing the complex spectra of metallic

surfaces. To help point out any useful trends in the inferred temperature, only errors below  $\pm 50$  K are given in the tables. Also, all wavelengths corresponding to the CO<sub>2</sub> and H<sub>2</sub>O bands are excluded from the analysis.

A first look at the results in Tables 4 and 5 shows only a small number of cases produce errors below 10 K, and the occurrence of these accurate measurements is rather random. Only one case produced an exact inferred temperature, namely the first-order LLE model over the 2.05-3.43  $\mu\text{m}$  range for AL 2024 with the roughened surface at 700 K.

However, the results do reveal some useful trends regarding preferred models and polynomial order. Both tables show “acceptable results” (designation used loosely here to denote temperature errors below  $\pm 50$  K) are concentrated mostly in the small wavelength range, although some previous studies suggest a large wavelength range can reduce temperature errors. In judging the suitability of a wavelength range, one has to examine how effectively an emissivity model can represent the actual emissivity distribution in that particular range. Tables 4 and 5 prove broadening the wavelength range to encompass all measured wavelengths makes it difficult for a particular mathematical function to accurately represent the emissivity distribution. This was demonstrated earlier by the complex shape of emissivity spectra in Fig. 5, 8, and 9.

Tables 4 and 5 show the LLE model yields inconsistent results. For example, although acceptable predictions are real-

**Table 5 Absolute Errors in Inferred Temperature of Al Alloys for Different Surface Roughness and Different Spectral Ranges at 700 K Using the LLE Model and LEM Model**

Surface Condition	Emissivity Model	Polynomial Order	Wavelength, $\mu\text{m}$								
			2.05-3.43			3.50-4.72			2.05-4.72		
			AL 1100	AL 2024	AL 7150	AL 1100	AL 2024	AL 7150	AL 1100	AL 2024	AL 7150
Polished	LLE	1	4.6	...	...	...	...	...	...	...	...
		2	...	...	...	...	...	...	...	...	...
		3	...	...	...	...	...	...	...	...	...
	LEM	1	...	-2.3	5.2	27.4	...	...	...	...	...
		2	35.5	...	...	...	...	...	...	47.4	...
		3	-11.6	...	25.1	...	...	...	34.6	...	...
Roughened with 14 $\mu\text{m}$ grit paper	LLE	1	-48.0	0.0	...	...	...	...	...	...	...
		2	...	...	...	...	...	...	...	...	...
		3	...	...	...	...	...	...	...	...	...
	LEM	1	-26.0	6.1	-14.6	...	...	-45.2	...	...	...
		2	...	...	...	...	...	...	-44.1	...	...
		3	32.9	-17.4	-10.6	...	...	...	...	-42.9	-34.7

Missing values correspond to errors beyond  $\pm 50$  K.

ized with the first-order LLE model for all three alloys over the short wavelength range for the polished surface at 600 K, only the AL 7150 shows acceptable results among the rough surfaces at 600 K. Results of the first-order LLE model are even less consistent at 700 K.

For the short-wavelength range at 600 K, Table 4 shows the third-order LEM model gives acceptable results for all three alloys as well as for both polished and roughened surfaces. Similar results are observed for the short wavelength range at 700 K, except for the polished AL 2024 surface. For the same wavelength range, the first-order LEM shows acceptable results for AL 2024 and AL 7150 at 700 K, but not at 600 K. Overall, the third-order LEM shows best overall compensation for the short wavelength range.

In general, similar results are realized with the LEM model for the different alloys since, as shown in Fig. 8(a), different alloys produce similar emissivity spectra. Changes in temperature and surface roughness, on the other hand, do not favor particular trends in emissivity spectra, as was indeed shown in Fig. 5 and 9, respectively. This proves further research is needed to develop more accurate models that are capable of handling the diverse operating conditions of Al processing plants.

## 5. Conclusions

In this study, experiments were performed to measure emissivity spectra for different Al surfaces subject to variations in alloy, temperature, heating time, and surface finish. The LEM and LLE models were tested for accuracy at inferring surface temperature subject to variations in the aforementioned parameters. Key findings from the study are discussed below.

For most metallic surfaces, spectral emissivity increases with decreasing wavelength. However, the present data exhibit a decreasing emissivity with increasing wavelength for  $\lambda < 3.5$   $\mu\text{m}$ , and the opposite trend for higher wavelengths.

Except for AL 1100 (commercially pure Al), the emissivity trends for all alloys are similar, first decreasing 600-700 K and

then increasing 700-800 K. The increased emissivity at 800 K is closely associated with a surface discoloration from light gray into black. For pure Al, the emissivity decreases monotonically with increasing temperature.

Heating time has the most effect on emissivity during the first 3 h for all alloys except AL 1100. Oxidation on the alloy surfaces appears to attain a consistent surface composition after 3 h, precluding further changes in emissivity.

Surface roughness alters the spectral emissivity substantially, resulting in 2- to 3-fold increases in emissivity for rough compared with polished surfaces, but the emissivity distribution becomes flatter with increased roughness.

When using the LLE and LEM models, acceptable results are concentrated mostly in the small wavelength range of 2.05-3.43  $\mu\text{m}$ ; broadening the wavelength range to encompass all measured wavelengths does not enhance measurement accuracy. Overall, the third-order LEM shows the best overall compensation for different alloys, temperatures, and surface roughness. The LLE model shows far less consistency in temperature accuracy.

The complex changes in spectral emissivity distribution resulting from temperature, alloy, and roughness emphasize the need for further research to develop more accurate models that are capable of handling the diverse operating environment of Al processing plants.

## Acknowledgments

The authors are thankful for the financial support of the Indiana 21<sup>st</sup> Century Research and Technology Fund. The authors also thank Mr. Gerry Dail of ALCOA for supplying Al samples for this study, and Dr. Jongmook Lim of Spectraline for his technical assistance.

## References

1. G.J. Dail, M.G. Fuhrman, and D.P. DeWitt: "Evaluation and Extension of the Spectral-Ratio Radiation Thermometry Method" in *Proc. 4th Int. Aluminum Extrusion Technology Seminar*, Vol. 2, Apr 11-14, 1988, pp. 281-86.

2. R. Siegel and J.R. Howell: *Thermal Radiation Heat Transfer*, McGraw-Hill, New York, 1972.
3. D.K. Edwards and I. Catton: "Advances in the Thermophysical Properties at Extreme Temperatures and Pressures" in *Proc. Symp. on Thermophysical Properties*, Mar 22-25, 1965, pp. 189-99.
4. P.B. Coates: "Multi-Wavelength Pyrometry," *Metrologia*, 1981, 17, pp. 103-09.
5. B.K. Doloresco: "Review of Multispectral Radiation Thermometry and Development of Constrained Minimization Method," M.S. Thesis, Purdue University, School of Mechanical Engineering, West Lafayette, IN, Dec 1986.
6. M.F. Hopkins: *Four Color Pyrometer for Metal Emissivity Characterization*, Vol 2599, SPIE—The International Society of Optical Engineering, Philadelphia, PA, 1996, pp. 294-301.
7. M.A. Khan, C.D. Allemand, and T.W. Eager: "Noncontact Temperature Measurement. II. Interpolation Based Techniques," *Rev. Sci. Instr.*, 1991, 62(2), pp. 403-09.
8. Th. Duvaut, D. Georgeault, and J.L. Beaudoin: "Multiwavelength Infrared Pyrometry: Optimization and Computer Simulations," *Infrared Phys. Technol.* 1995, 36, pp. 1089-09.
9. J.L. Gardner, T.P. Jones, and M.R. Davies: "A Six-Wavelength Radiation Pyrometer," *High Temperatures—High Pressures*, 1981, 13, pp. 459-66.
10. J.L. Gardner: "Computer Modeling of Multiwavelength Pyrometer for Measuring True Surface Temperature," *High Temperatures—High Pressures*, 1980, 12, pp. 699-705.
11. G.B. Hunter, C.D. Allemand, and T.W. Eager: "Prototype Device for Multiwavelength Pyrometer," *Optical Eng.*, 1986, 25(11), pp. 1222-31.
12. M.A. Khan, C.D. Allemand, and T.W. Eager: "Noncontact Temperature Measurement. I. Interpolation Based Techniques," *Rev. Sci. Instr.*, 1991, 62(2), pp. 392-402.
13. M.A. Khan: "Non-Contact Temperature Measurement," Ph.D. Thesis, Massachusetts Institute of Technology, Materials Engineering, Cambridge, MA, 1988.
14. M. Battuello, T. Ricolfi, and L. Wang: "Use of a Photodiode-array Spectroscopic System for Temperature Measurement" in *Proc. of TEMPMEKO '93: 5th Int. Symp. on Temperature and Temperature Measurement in Industry and Science*, 1993, pp 150-55.
15. G.R. Gathers: "Analysis of Multiwavelength Pyrometry Using Non-linear Chi-Square Fits and Monte Carlo Methods," *Int. J. Thermophys.*, 1992, 13(3), pp. 539-54.
16. M. Hoch: "The Integral Six-Color Pyrometer: A New General Method of Temperature Determination," *High Temperatures—High Pressures*, 1992, 24, pp. 607-23.
17. M. Hoch: "The Integral Six-Color Pyrometer: Linear Dependence of the Radiance Temperature  $T_r$  on the Wavelength  $\lambda$ ," *Rev. Sci. Instr.*, 1992, 63(4), pp. 2274-81.
18. G.R. Gathers: "Monte Carlo Studies of Multiwavelength Pyrometry Using Linearized Equations," *Int. J. Thermophys.*, 1992, 13(2), pp. 361-82.
19. G.R. Gathers: "Analysis of Multiwavelength Pyrometry Using Non-linear Chi-Square Fits and Monte Carlo Methods," *Int. J. Thermophys.*, 1992, 13(3), pp. 539-54.
20. M.A. Pellerin, D.P. DeWitt, and G.J. Dail: "Multispectral Radiation Thermometry for Aluminum Alloys" in *Heat Transfer in Metals and Containerless Processing and Manufacturing*, T.L. Bergman, D.A. Zumbrennen, Y. Bayazitoglu, and A.G. Lavine, ed., *ASME Heat Transfer Division*, 1991, 162, pp. 43-47.
21. F.P. Incropera and D.P. DeWitt: *Fundamentals of Heat and Mass Transfer*, 4th ed., John Wiley and Sons, New York, 1996, p. 657.
22. M.J. Haugh: "Radiation Thermometry in the Aluminum Industry" in *Theory and Practice of Radiation Thermometry*, D.P. DeWitt and G.D. Nutter, ed., John Wiley and Sons, New York, 1988.
23. M.A. Pellerin, B.K. Tsai, D.P. DeWitt, and G.J. Dail: "Emissivity Compensation Method for Aluminum Alloy Temperature Determination" in *Temperature, Its Measurement and Control in Science and Industry*, Vol 6, Part 2, J.F. Schooley, ed., American Institute of Physics, New York, 1992, pp. 871-76.
24. B.K. Tsai, R.L. Shemaker, D.P. DeWitt, B.A. Cowans, Z. Dardas, W.N. Delgass, and G.J. Dail: "Dual-Wavelength Radiation Thermometry: Emissivity Compensation Algorithms," *Int. J. Thermophys.*, 1990, 11(1), pp. 269-81.